Langmuir

Article

pubs.acs.org/Langmuir

Scattering Function for Branched Wormlike Chains

Karsten Vogtt,*,† Gregory Beaucage,*,† Michael Weaver,‡ and Hanqiu Jiang†

†CEAS-Biomedical, Chemical, and Environmental Engineering, University of Cincinnati, Cincinnati, Ohio 45221, United States

‡P&G Analytical Sciences, 8700 Mason-Montgomery Road, Mason, Ohio 45040, United States

ABSTRACT: Wormlike or threadlike structures with local cylindrical geometry are abundantly found in nature and technical products. A thorough structural characterization in the bulk for a whole ensemble, however, is difficult. The inherent semiordered nature of the tortuous large-scale structure and especially the quantification of branching renders an assessment difficult. In the present work we introduce a hybrid function expressing the scattering intensities for X-rays, neutrons, or light in the small-angle regime for this system. The function is termed "hybrid" because it employs terms from different approaches. The large-scale structure is described via a Guinier term as well as a concomitant power-law expression in momentum transfer q taken from the so-called unified function. The local cylindrical shape, however, is taken into account through a form factor for cylinders from rigid-body modeling. In principle, the latter form factor can be replaced by an expression for any other regular body so that the new hybrid function is a versatile tool for studying hierarchical structures assembled from uniform subunits. The appropriateness and capability of the new function for cylindrical structures is exemplified using the example of a wormlike micellar system.

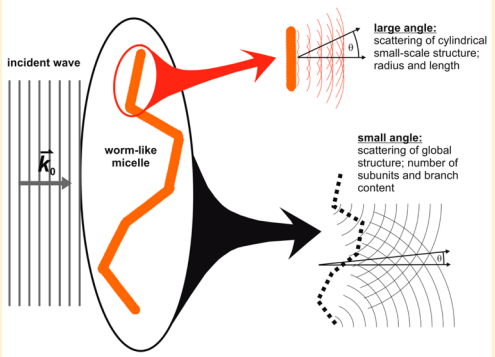

INTRODUCTION

Fibrous assemblies in technical products or the cytoskeleton in biological cells are just a few examples of structures which can be termed wormlike or threadlike. This ubiquitous structural motif determines the macroscopic properties of these materials, in particular, mechanical properties such as elasticity or viscosity. A thorough assessment of the underlying structural features is of crucial importance to understanding these phenomena within the paradigm of structure−function relationships.

A first description of threadlike molecules in terms of X-ray scattering was given as early as 1949.[1] Here the smoothly curved thread or wormlike particle is comprehended as a chain of elongated, cylindrical segments giving rise to a description as wormlike chains (WLCs).[2−4] Thus, WLCs can be formally treated similarly to polymer molecules and can be characterized via the well-known persistence length l_p and the Kuhn length $l_K = 2l_p$ (for infinite, linear, Gaussian chains). The Kuhn length is associated with the step length in the freely jointed chain model, while the persistence length is associated with statistical persistence in the wormlike chain model. For stiff, rigid cylindrical segments the length of the cylinder or rod can be identified with l_k.[5] In biology l_p adapts values from tens of nanometers for DNA,[6,7] over tens of micrometers for actin,[8,9] to the millimeter range for microtubules.[10] It has been demonstrated that a DNA molecule exhibits properties of a wormlike chain, while mixtures of actin-binding protein and actin resemble covalently cross-linked networks.[6,11] For synthetic products, l_p can vary from a few Ångstrom for polymers in a solution or melt,[12] over a few or tens of nanometers for polyelectrolytes,[13] and up to hundreds of nanometers for carbon nanotubes.[14] Within the Gaussian chain model the value k_BT $(3\langle R^2\rangle/2zl_k^2)$ is directly related to the energy of a stretched molecule (where k_B is the Boltzmann constant, T the absolute temperature, $\langle R^2\rangle$ is the mean square end-to-end distance, and z is the number of subunits of length l_k). In solution, WLCs and their structure are thus closely related to the viscoelastic properties of the liquid.

The connection between rheology and microscopic structure is of special interest for micellar systems, which can be assembled from various amphiphilic molecules such as surfactants and (block) copolymers and which exhibit a wide and diverse range of structures.[15−20] WLCs formed by micelles are called wormlike micelles (WLMs). These can grow to aspect ratios exceeding several thousand and can exhibit branching.[21−23] The importance of their rheological properties is underlined by the utilization of WLMs in thickeners, drag reducers, or fracking fluids in the petrochemical industry.[24,25] An interesting feature of surfactant WLMs is that with increasing surfactant concentration or salt concentration the zero shear-rate viscosity often reaches a peak and decreases. As an explanation of this phenomenon it has been suggested that the appearance of branches at high salt or surfactant concentrations allows for faster relaxation.[26,27] The rheology of WLMs has been intensively studied, and the elucidation of the structure−function relationship for this system is a major aim of recent research.[27−35] Small-angle neutron scattering (SANS) was employed for the structural characterization in

Received: November 17, 2014
Revised: June 28, 2015
Published: July 7, 2015

DOI: 10.1021/acs.langmuir.5b01630
Langmuir 2015, 31, 8228−8234

these works. For surfactants with an aliphatic hydrophobic tail, contrast is enhanced over the comparable technique of X-ray scattering by a factor of hundreds to thousands through the use of deuterated water.

Several works have elaborated functions for the analysis of small-angle scattering data from wormlike micellar systems.[36−39] However, none of them account for the presence of branches. Foster et al. developed a scattering function for a network of junctions,[40] but this approach is restricted to dense networked systems such as bicontinuous sponge phases. Branching, however, is frequently found in polymeric and amphiphilic systems.[41,42] It is of crucial importance to the rheological behavior in the case of WLMs.[27,28] Moreover, for an utmost general description of WLCs, the implementation and quantification of branching are required.

We therefore developed a hybrid scattering function which accounts for the local cylindrical geometry as well as for the large-scale, global structure including branching. The scattering contribution of the cylindrical subunits is expressed via a form factor for cylinders,[43] while the scattering intensity stemming from the overall distribution of these subunits within the WLC is taken from a unified Guinier/power law approach developed by Beaucage.[44] In the Theory section a detailed description of this hybrid function is given. The Results section depicts the application of the hybrid function using the example of a mixed surfactant WLM system consisting of the two surfactants monoethoxylated sodium laureth sulfate (SLE1S) and cocamidopropyl betaine (CAPB).

THEORY

With the unified Guinier/power law approach an arbitrary number of structural hierarchies can be described. Hereby each level of structure is described via a Guinier and a power law term. The overall scattering intensity $I(q)$ is given by the sum of all of these contributions[44]

$$I(q) = \sum_i \left(G_i e^{-R_{g,i}^2 q^2/3} + B_i e^{-R_{g,i-1}^2 q^2/3} (q^*)^{-d_{f,i}}\right) \tag{1}$$

where[45]

$$q^* = \frac{q}{\mathrm{erf}\left(\frac{q 1.06 R_{g,i}}{\sqrt{6}}\right)^3} \tag{2}$$

defining $\mathrm{erf}(x)$ as the error function. The index i denotes a level within the structural hierarchy. i has the lowest value for the smallest structural level. q is the modulus of momentum transfer and is equal to $4\pi/\lambda \sin(\theta/2)$, with λ being the wavelength and θ being the scattering angle of the radiation. G_i is the corresponding scattering contribution for structural level i at zero angle, $R_{g,i}$ is the respective radius of gyration, and $d_{f,i}$ is the fractal dimension. Two adjacent structural levels are connected via $R_{g,i-1}$ in the power law term which serves to cut off the low-q power law. The expression for amplitude B_i of the power law term can vary depending on the type of system. For polydisperse fractal objects the following relation can be applied:[46]

$$B_i = G_i \frac{C_p d_{\min,i}}{R_{g,i}^{d_{f,i}}} \Gamma\left(\frac{d_{f,i}}{2}\right) \tag{3}$$

Here, $\Gamma(x)$ is the gamma-function and C_p is a chain polydispersity factor, a measure for polydispersity of mass z. The latter value can be calculated via $d_{f,i}$ according to Sorensen and Wang.[45,47] For $d_f = 2$ the factor C_p is given by M_z/M_w. The parameter d_{min} is the so-called minimum path dimension, i.e., the fractal dimension of the average, minimum path (or short circuit path) through a given structure. For linear chains, $d_{min} = d_f$. The ratio of d_f/d_{min} is termed the connectivity dimension c. For a regular body such as a sphere or a disc, $d_{min} = 1$ and $d_f = c$. For a linear chain in good solvent $d_{min} = d_f = 5/3$ and $c = 1$.[46] For a low branch content $n_{br} < 1$, i.e., with an average amount of less than one branch per WLC, one may approximate $d_{min} \approx 5/3$ for a self-avoiding walk, and n_{br} is obtained from the following relation[45]

$$n_{br} = \frac{z^{\left[\left(\frac{5}{2d_f} - \frac{3}{2c}\right) + \left(1 - \frac{1}{c}\right)\right]} - 1}{2} \tag{4}$$

where z is the number of subunits (see text below eq 6). With the above formalism the scattering intensity $I(q)$ of an arbitrary number of structural levels can be expressed. For the hybrid function approach, the lowest structural level $i = 1$ according to eq 1 is not expressed with the given Guinier/power law terms. The contribution $I_1(q)$ of the first level, corresponding to the smallest structural "building" unit of the model, is expressed through a form factor $P_{cyl}(q)$ for a cylinder according to the local cylindrical symmetry of the WLCs:[43]

$$I_1(q) = \int_0^\infty N(R_1)\, G_1 P_{cyl}(q, R_1, L_1)\, \mathrm{d}R_1 \tag{5}$$

In present case the radius R_1 of the cylindrical subunits is considered to be polydisperse, which is taken into account via a distribution function $N(R_1)$. L_1 is the length of the cylindrical subunits. In the freely jointed chain model the step length is the Kuhn length, l_k. Because the cylindrical subunit resembles such a step length, we associate L_1 with l_k. In the following, form-factor-derived symbol L_1 is retained because this interpretation may be subject to some debate. The value $G_1 = I_1(0)$ is given by $N/V(\Delta\rho)^2 V_{cyl}^2$, where N/V is the number density, $V_{cyl} = (\pi R_1^2 L_1)$ is the volume of the cylinders, and $\Delta\rho$ is the difference in the scattering length density ρ_{cyl} of the cylinders and that of the solvent ρ_s. Note that in principle the form factor $P(q)$ of any regular body can be employed here for the description of the local structure.

For WLCs, structural level $i = 2$ can be identified with the tortuosity and branching of the interconnected subunits. The corresponding scattering contribution $I_2(q)$ can be formulated according to eq 1. The radius of gyration $R_{g,1}$ required for this is given by the radius of gyration for a cylinder $R_{g,1}^2 \approx L_1^2/12 + R_1^2/2$, where R_1 is approximated by the moment of the distribution in eq 5. If no further superstructure needs to be taken into account, then the overall scattering intensity $I(q)$ is given by the sum of $I_1(q)$ and $I_2(q)$:

$$I(q) = I_1(q) + I_2(q) \tag{6}$$

With eq 6 the scattering intensity of diluted solutions of WLCs can be fitted. In this case the number of subunits is $z = G_2/G_1 + 1$. Because small spatial correlations dominate the scattering to large scattering angles θ (Figure 1), $I_1(q)$ dominates $I(q)$ at high q while $I_2(q)$ dominates the low-q region. Figure 2 depicts a theoretical $I(q)$, for example, and highlights characteristic features and their connection to the variables defined above. It is advised to start the fitting procedure with a fit of $I_1(q)$ to the high-q region to obtain the starting values for the fit of the $i = 1$ parameters. In the next

DOI: 10.1021/acs.langmuir.5b01630
Langmuir 2015, 31, 8228−8234

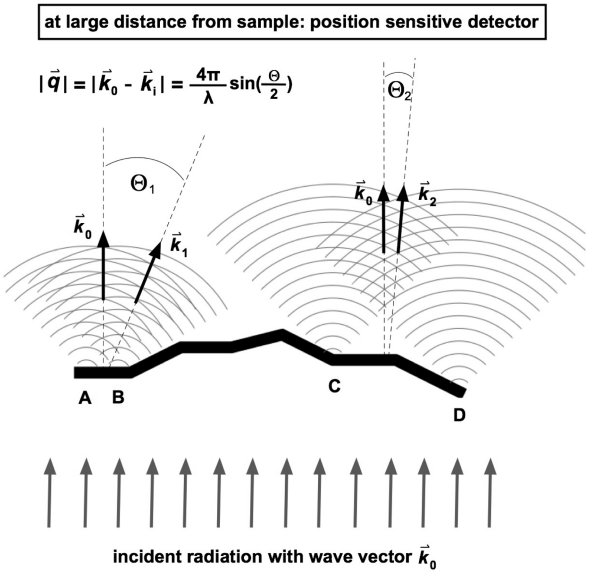

Figure 1. Simplified principle of a neutron scattering experiment and the separation into large-range and small-range correlations for WLMs.

step, a fit of the whole q range with all fitting parameters $i = \{1, 2\}$ can be attempted.

EXPERIMENTAL SECTION

The surfactant mixtures were made by combining 70 wt % active sodium laureth-1-sulfate paste (SLE1S, CAS no. 68585-34-2) and 30 wt % active cocoamidopropyl betaine (CAPB, CAS no. 61789-40-0). The surfactants are typical personal care product industrial surfactants commercially available from Stepan (Northfield, IL); these feature a comparatively narrow distribution of chain lengths (~68:25 C12−C14) and ethoxylation for SLE1S (1 mol of EO). Weight ratios of SLE1S/CAPB of between 11:1 and 8:1 gave essentially the same qualitative viscosity−salt curve behavior with only small differences in the maximum viscosity attained, so a fixed 8.65:1 weight ratio was chosen for this work. Prior to mixing the surfactants, the activity of the SLE1S paste was verified using the potentiometric anionic surfactant titration ASTM D4251 procedure. A Mettler TX70 autotitrator with Mettler DS500 tenside and DX200 reference electrodes was used. A similar approach was used for CAPB using sodium tetraphenylborate as the titrant.[48] Likewise, autotitration procedures from AOCS were used to measure the Na_2SO_4 (Dc7-59) and NaCl (DB 7b-55) contents, respectively. A Mettler DMC 141SC silver electrode was used for the NaCl titration; for Na_2SO_4, a Mettler DMC 140SC platinum electrode was employed. The samples were prepared in D_2O (Cambridge Isotopes, 99.96%) with NaCl added to the concentrations specified. The background corrections for SANS experiments used NaCl/D_2O solutions at the same concentration. Flow viscosity measurements were made either using a TA Instruments DHR3 rheometer with cup and bob geometry or an Anton Paar Lovis ME2000 rolling ball viscometer. For DHR3, the temperature was controlled using a Peltier cup accessory and a solvent trap was used to maintain the environmental integrity. The viscosity flow curves were collected using TRIOS software using steady-state sensing, and the zero shear viscosity was verified by measuring over several shear rate settings below 0.1 s^{-1} to verify the zero-shear viscosity plateau at shear rates below the onset of the shear-thinning region. The reported zero shear viscosity was typically the average of several viscosity data points between 0.001 and 0.01 s^{-1}.

SANS data was measured on the Bio-SANS instrument at Oak Ridge National Laboratory, Oak Ridge, Tennessee, USA. Macros for the Igor Pro software provided by the beamline were employed for data reduction. The reduced and background-corrected data was fitted using eq 6. $I_2(q)$ was defined as given in eqs 1−3, and for $I_1(q)$ the following expression was used

$$I_1(q) = \phi_V(\Delta\rho)^2 \frac{\int_0^\infty R_1^2 N(R_1)\, V_{cyl} P_{cyl}(q, R_1, L_1)\, dR_1}{\int_0^\infty R_1^2 N(R_1)\, dR_1} \quad (7)$$

where $\phi_V = NV_{cyl}/V$ is the volume fraction. The separation of V_{cyl} from the integral is corrected by the introduction of R_1^2 in the numerator integral and the corresponding normalization. For $P_{cyl}(q, R_1, L_1)$ a quick numerical approximation was employed following the formula given in the SASfit software manual.[49] A log-normal distribution function $N(R_1)$ described the polydispersity of the cylinder radii. In the following text R_1 denotes the corresponding median value and $\sigma_{R,1}$ denotes the geometric standard deviation.

RESULTS

Figure 3 depicts the scattering intensity $I(q)$ of 0.232% of mixed surfactant at various salt concentrations. Fits according to eq 6 are given as gray lines. The obtained fitting parameters are given in Table 1. The volume fraction of the samples was 0.0024, yielding an average scattering length density of $-(0.3 \pm 0.1) \times 10^{10}$ cm^{-2} (assuming a scattering length density of 6.4×10^{10} cm^{-2} for the solvent D_2O). The value is smaller than the expected one of about $+0.3 \times 10^{10}$ cm^{-2} based on the composition and density. Possibly the main scattering stems from a dense hydrocarbon core exhibiting negative scattering length densities, while the hydrated headgroups contribute less to the overall contrast. A fit as a cylindrical shell would probably

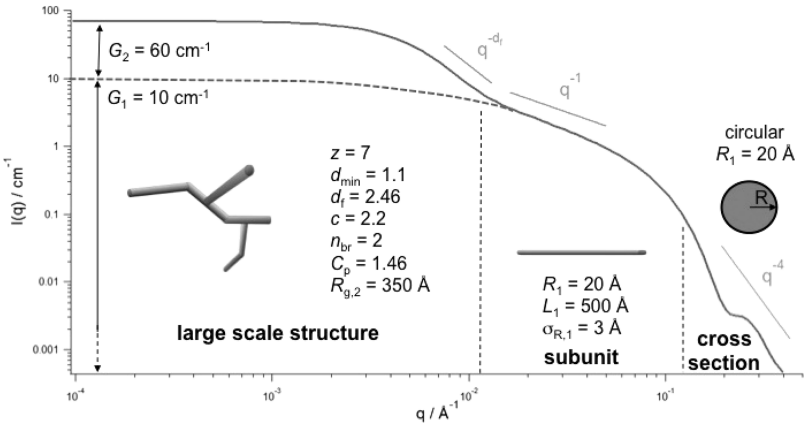

Figure 2. Theoretical example $I(q)$ with highlighted spatial regimes. The dashed gray line denotes the contribution $I_1(q)$. For an explanation of the variables refer to the text.

DOI: 10.1021/acs.langmuir.5b01630
Langmuir 2015, 31, 8228−8234

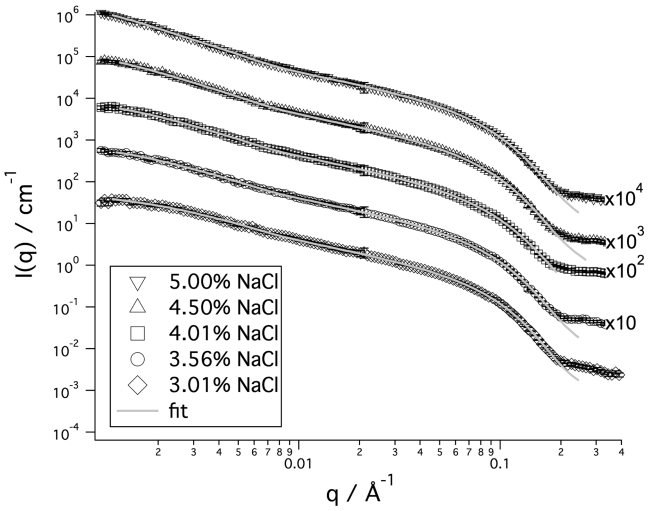

Figure 3. Scattering intensity $I(q)$ and fits for 0.232 wt % of the mixed surfactant at various salt concentrations. The data points were shifted along the y axis for better visibility.

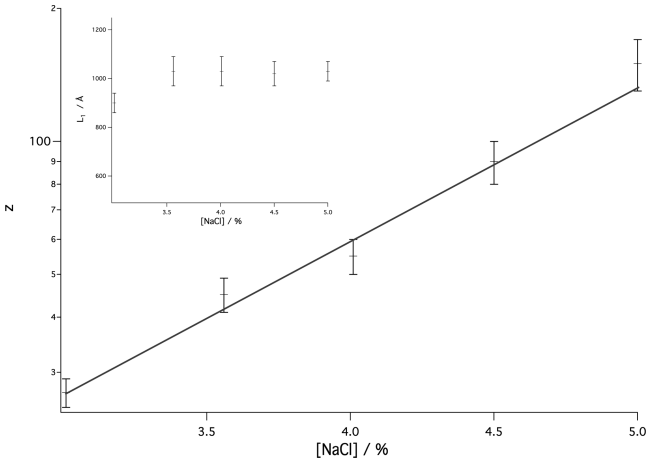

Figure 4. Semilogarithmic plot of z vs salt concentration for 0.232 wt % of the mixed surfactant in D_2O. The inserted gray line is a guide for the eye only. The inset depicts the change of L_1 with salt concentration.

be a more appropriate model. (See the discussion of the high-q region below.)

The changes in $I(q)$ with salt concentration at intermediate and high q are small, indicating just small structural changes with respect to the cylindrical subunits. Large changes are seen, however, at low q. This demonstrates that the structural impact of salt in the observed concentration range mainly affects the large-scale structure. Indeed L_1 just changes slightly with the variation of [NaCl] (Figure 4 inset). Similar behavior has been found by Magid et al. for sodium dodecyl sulfate micelles, where the Kuhn length varies less than 10% for about 0.23 wt % surfactant between 7 and 11.6 wt % NaCl.[50] They find substantially lower Kuhn lengths, which is probably due to the different kind of surfactant used as well as to the higher salt concentrations employed. The latter reduce the Coulomb repulsions, which in turn decrease the stiffness or rigidity of the subunits and the corresponding electrostatic contribution to l_K.[51]

At the highest q the fits and the data points differ considerably. Here probably the approximation of a homogeneous cylinder cross-section with a log-normal distribution of radii reaches its limit. Accordingly the fitting values reported for the radius are just of an approximate nature, and error margins are denoted just for the sake of completeness. Deviations between data points and the fit at high q have already been reported for cetyltrimethylammonium bromide micelles.[52] In general, it has to be noted that standard deviations obtained from multiparameter fits do not provide a measure for the amount of other physically meaningful parameter sets which likewise would fit the data points in a satisfactory manner. They just denote a measure of the difference between the best fit and the given data points rather than attesting to its uniqueness. This is an inherently mathematical problem. The low error margins for fitting parameter $i = 1$ demonstrate that the fitting function describes the data points remarkably well in the chosen q region rather than reflecting the true accuracy in real space. The underlying model assumes homogeneous cylinders with a smooth interface. Thus, the lower spatial limit, which reasonably can be considered, is in the Ångstrom regime for the present system.

The curvature of $I(q)$, i.e., the power law at low q, hardly changes; just the scattering intensity at zero angle G_2 increases steadily with increasing salt concentration. This finding indicates that the large-scale structure grows via an increase in the number of subunits z upon addition of NaCl, in agreement with results from other works.[28] Figure 4 depicts a plot of z vs salt concentration [NaCl]. The number of subunits increases in a roughly exponential manner with the amount of added salt. The specific viscosity $\eta_{sp} = (\eta - \eta_0)/\eta_0$ vs L_2 is depicted in Figure 5, where η is the viscosity of the surfactant solution and η_0 is the respective value for the solvent. The dependence of η_{sp} on L_2 can be well described with a power law

Table 1. Fitting Parameters as Well as z and n_{br} for 0.232 wt % of the Mixed Surfactant under Various Salt Conditions in D_2O[a]

	3.01% NaCl	3.56% NaCl	4.01% NaCl	4.5% NaCl	5.0% NaCl
$\phi(\Delta\rho)^2/(10^{19}\ \mathrm{cm}^{-4})$	1.052 ± 0.003	1.070 ± 0.003	1.122 ± 0.004	1.053 ± 0.003	1.063 ± 0.003
R_1/Å	16.46 ± 0.09	15.87 ± 0.09	15.16 ± 0.09	16.32 ± 0.09	16.18 ± 0.09
$\sigma_{R,1}$/Å	1.29 ± 0.01	1.324 ± 0.004	1.354 ± 0.004	1.323± 0.004	1.335 ± 0.004
L_1/Å	900 ± 40	1030 ± 60	1030 ± 60	1020 ± 50	1030 ± 40
G_2/cm^{-1}	50 ± 5	95 ± 9	120 ± 10	200 ± 20	330 ± 40
$R_{g,2}$/Å	1500 ± 500	2000 ± 500	1900 ± 500	2200 ± 400	2600 ± 400
$d_{f,2}$	1.7 ± 0.2	1.7 ± 0.2	1.8 ± 0.2	1.8 ± 0.1	1.88 ± 0.08
z	27 ± 2	45 ± 4	55 ± 5	90 ± 10	150 ± 20
n_{br}	0.1 ± 0.4	0.1 ± 0.4	0.2 ± 0.4	0.3 ± 0.4	0.4 ± 0.3

[a]The value of $d_{min,2}$ was set to 1.67 for all samples assuming a self-avoiding walk for the cylindrical subunits. Parameters z and n_{br} are derived and calculated as described in the Theory section.

DOI: 10.1021/acs.langmuir.5b01630
Langmuir 2015, 31, 8228−8234

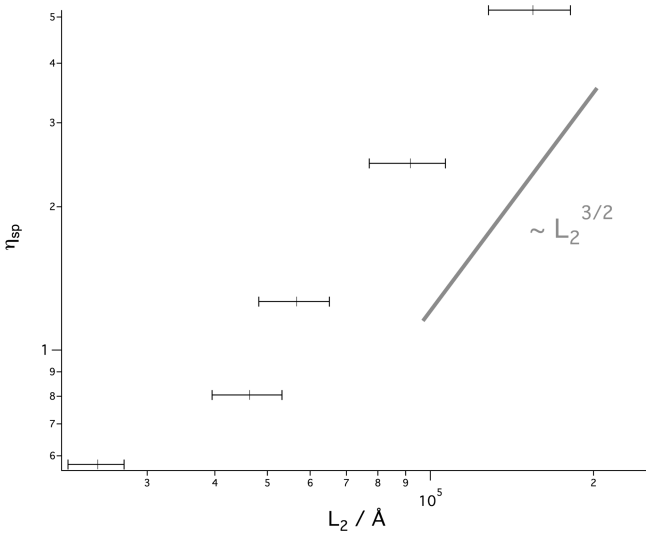

Figure 5. Plot of the specific viscosity η_{sp} vs contour length L_2. The gray line depicts a power law fit with a fixed exponent of 3/2.

term using an exponent of 3/2 as predicted for the diluted regime.[53]

For most of the examined salt concentrations the branch content n_{br} is indistinguishable from zero (Figure 6). The error

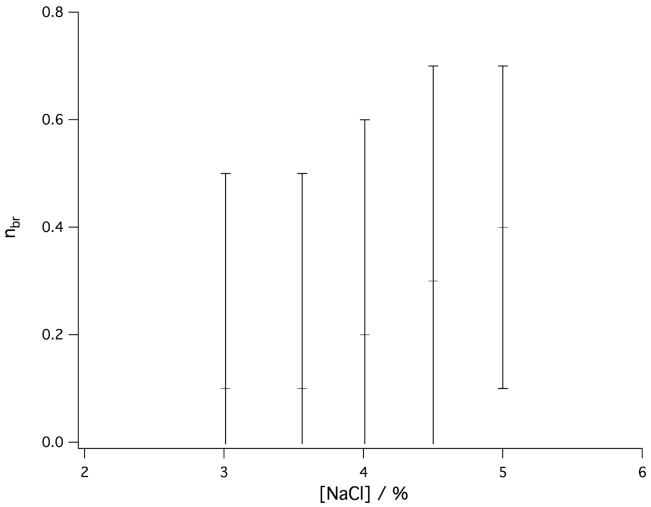

Figure 6. Change in branch content n_{br} with salt concentration.

bars for the parameters of the global structure are large because the lower q limit of the experiment lies above the Guinier region of the overall assembly. Accordingly, the fit parameters as well as the values calculated from these via error propagation exhibit large inaccuracies. For an improved determination of these parameters complementary ultra-small-angle neutron scattering or small-angle light scattering experiments are required. Nonetheless a clear trend toward larger branch content is visible with increasing salt concentration. At 5 wt % NaCl, $n_{br} = 0.4 \pm 0.3$ is distinguishable from zero. This value denotes the number of branches per WLM, the reciprocal value according to the number of WLMs per branch, which for cases of $n_{br} < 1$ is more instructive. Hence on average every 10th to roughly every 2nd WLM contains a single branch in the above case.

All in all the new scattering function yields results in agreement with the literature data. An enlargement of the overall WLM structure with increasing salt concentration is observed. Moreover the presence of branches at 5 wt % NaCl has been demonstrated in these measurements. The developed model is comparatively simple, can be applied to all WLC systems, and takes branching into account. Moreover, the employed form factor for the description of the smallest structural unit ($i = 1$) can be freely chosen. Thus, in principle a broad variety of local geometries can be accounted for, just limited by the availability of corresponding form factors $P(q)$. For branched and/or tortuous networks from the nanometer to the micrometer scale, the newly developed hybrid function allows a quick and robust assessment of local and global structure.

SUMMARY

A hybrid unified scattering function has been developed for the modeling of tortuous and/or branched structures in the important spatial range from nanometers to micrometers. The function is a hybrid of a form factor for cylinders to account for local geometry and a term from the unified function to describe the global structure. Besides being a relatively simple algorithm it allows the detection and quantification of branching. Using the example of surfactant WLMs, the effect of salt on size and branch content has been demonstrated.

AUTHOR INFORMATION

Corresponding Authors

*E-mail: vogttkn@.uc.edu.
*E-mail: gregory.beaucage@uc.edu.

Author Contributions

The manuscript was written through the contributions of all authors. All authors have given approval to the final version of the manuscript.

Notes

The authors declare no competing financial interest.

ACKNOWLEDGMENTS

Research conducted at ORNL's High Flux Isotope Reactor was sponsored by the Scientific User Facilities Division, Office of Basic Energy Sciences, U.S. Department of Energy.

REFERENCES

(1) Kratky, O.; Porod, G. Röntgenuntersuchung gelöster Fadenmoleküle. *Rec. Trav. Chim. Pays-Bas* **1949**, *68*, 1106−1123.
(2) Fixman, M.; Kovac, J. Polymer conformational statistics. III. Modified gaussian models of stiff chains. *J. Chem. Phys.* **1973**, *58*, 1564−1568.
(3) Marko, J. F.; Siggia, E. D. Stretching DNA. *Macromolecules* **1995**, *28*, 8759−8770.
(4) Bouchiat, C.; Wang, M. D.; Allemand, J.-F.; Strick, T.; Block, S. M.; Croquette, V. Estimating the Persistence Length of a Worm-Like Chain Molecule from Force- Extension Measurements. *Biophys. J.* **1999**, *76*, 409−413.
(5) Flory, P. J. Statistical Thermodynamics of Mixtures of Rodlike Particles. 6. Rods Connected by Flexible Joints. *Macromolecules* **1978**, *11*, 1141−1144.
(6) Bustamante, C. Entropic elasticity of λ-phage DNA. *Science* **1994**, *265*, 1599−1600.
(7) Smith, S. B.; Finzi, L.; Bustamante, C. Direct mechanical measurements of the elasticity of single DNA molecules by using magnetic beads. *Science* **1992**, *258*, 1122−1126.

DOI: 10.1021/acs.langmuir.5b01630
Langmuir 2015, 31, 8228−8234

(8) Janmey, P. A.; Hvidt, S.; Käs, J.; Lerche, D.; Maggs, A.; Sackmann, E.; Schliwa, M.; Stossel, T. P. The mechanical properties of actin gels. *J. Biol. Chem.* **1994**, *269*, 32503−32513.
(9) Ott, A.; Magnasco, M.; Simon, A.; Libchaber, A. Measurement of the persistence length of polymerized actin using fluorescence microscopy. *Phys. Rev. E: Stat. Phys., Plasmas, Fluids, Relat. Interdiscip. Top.* **1993**, *48*, R1642−R1645.
(10) Pampaloni, F.; Lattanzi, G.; Jonás, A.; Surrey, T.; Frey, E.; Florin, E.-L. Thermal fluctuations of grafted microtubules provide evidence of a length-dependent persistence length. *Proc. Natl. Acad. Sci. U.S.A.* **2006**, *103*, 10248−10253.
(11) Janmey, P. A.; Hvidt, S.; Lamb, J.; Stossel, T. P. Resemblance of actin-binding protein/actin gels to covalently crosslinked networks. *Nature* **1990**, *345*, 89−92.
(12) Kienberger, F.; Pastushenko, V. P.; Kada, G.; Gruber, H. J.; Riener, C.; Schindler, H.; Hinterdorfer, P. Static and Dynamical Properties of Single Poly(Ethylene Glycol) Molecules Investigated by Force Spectroscopy. *Single Mol.* **2000**, *1*, 123−128.
(13) Tricot, M. Comparison of experimental and theoretical persistence length of some polyelectrolytes at various ionic strengths. *Macromolecules* **1984**, *17*, 1698−1704.
(14) Sano, M.; Kamino, A.; Okamura, J.; Shinkai, S. Ring closure of carbon nano tubes. *Science* **2001**, *293*, 1299−1303.
(15) Rehage, H.; Hoffmann, H. Viscoelastic surfactant solutions: model systems for rheological research. *Mol. Phys.* **1991**, *74*, 933−973.
(16) de Graaf, A. J.; Boere, K. W. M.; Kemmin, J.; Fokkink, R. G.; van Nostrum, C. F.; Rijkers, D. T. S.; van der Gucht, J.; Wienk, H.; Baldus, M.; Mastrobattista, E.; Vermonden, T.; Hennink, W. E. Looped structure of flowerlike micelles revealed by 1H-NMR relaxometry and light scattering. *Langmuir* **2011**, *27*, 9843−9848.
(17) Shrestha, R. G.; Nomura, K.; Yamamoto, M.; Yamawaki, Y.; Tamura, Y.; Sakai, K.; Sakamoto, K.; Sakai, H.; Abe, N. Peptide-based Gemini amphiphiles: Phase behavior and rheology of wormlike micelles. *Langmuir* **2012**, *28*, 15472−15481.
(18) Lee, H. L.; Adhimoolam Arunagirinathan, M.; Vagias, A.; Lee, S.; Bellare, J. R.; Davis, H. T.; Kaler, E. W.; McCormick, A. V.; Bates, F. S. Almost fooled again: New insights into cesium dodecyl sulfate micelle structures. *Langmuir* **2014**, *30*, 12743−12747.
(19) Jain, S.; Bates, F. S. On the origin of morphological complexity in block copolymer surfactants. *Science* **2003**, *300*, 460−464.
(20) Walther, A.; Goldmann, A. S.; Yelamanchili, R. S.; Drechsler, M.; Schmalz, H.; Eisenberg, A.; Müller, A. H. E. Multiple morphologies, phase transitions, and cross-linking of crew-cut aggregates of polybutadiene-*block*-poly(2-vinylpyridine) diblock copolymers. *Macromolecules* **2008**, *41*, 3254−3260.
(21) Chu, Z.; Feng, Y.; Su, X.; Han, Y. Wormlike micelles and solution properties of C22-tailed amidosulfobetaine surfactant. *Langmuir* **2010**, *26*, 7783−7791.
(22) Lin, Z. Branched Wormlike micelles and their networks. *Langmuir* **1996**, *12*, 1729−1737.
(23) Ziserman, L.; Abezgauz, L.; Ramon, O.; Raghavan, S. R.; Danino, D. Origins of the viscosity peak in wormlike micellar solutions. 1. Mixed catanionic surfactants. A cryo-transmission electron microscopy study. *Langmuir* **2009**, *25*, 10483−10489.
(24) Ezrahi, S.; Tuval, E.; Aserin, A. Properties, main applications and perspectives of worm micelles. *Adv. Colloid Interface Sci.* **2006**, *128*−*130*, 77−102.
(25) Yang, J. Viscoelastic wormlike micelles and their applications. *Curr. Opin. Colloid Interface Sci.* **2002**, *7*, 276−281.
(26) Lequeux, F. Reptation of connected wormlike micelles. *Europhys. Lett.* **1992**, *19*, 675−681.
(27) Rogers, S. A.; Calabrese, M. A.; Wagner, N. J. Rheology of branched wormlike micelles. *Curr. Opin. Colloid Interface Sci.* **2014**, *19*, 530−535.
(28) Dreiss, C. A. Wormlike micelles: where do we stand? Recent developments, linear rheology and scattering techniques. *Soft Matter* **2007**, *3*, 956−970.
(29) Helgeson, M. E.; Reichert, M. D.; Hu, Y. T.; Wagner, N. J. Relating shear banding, structure and phase behavior in wormlike micellar solutions. *Soft Matter* **2009**, *5*, 3858−3869.
(30) Helgeson, M. E.; Hodgdon, T. K.; Kaler, E. W.; Wagner, N. J. Formation and rheology of viscoelastic "double networks" in wormlike micelle-nanoparticle mixtures. *Langmuir* **2010**, *26*, 8049−8060.
(31) Liberatore, M. W.; Nettesheim, F.; Vasquez, P. A.; Helgeson, M. E.; Wagner, N. J.; Kaler, E. W.; Cook, L. P.; Porcar, L.; Hu, Y. T. Microstructure and shear rheology of entangled wormlike micelles in solution. *J. Rheol.* **2009**, *53*, 441−458.
(32) Helgeson, M. E.; Vasquez, P. A.; Kaler, E. W.; Wagner, N. J. Rheology and spatially resolved structure of cetyltrimethylammonium bromide wormlike micelles through the shear banding transition. *J. Rheol.* **2009**, *53*, 727−756.
(33) Lodge, T. P.; Taribagil, R.; Yoshida, T.; Hillmyer, M. A. SANS evidence for the cross linking of wormlike micelles by a model hydrophobic ally modified polymer. *Macromolecules* **2007**, *40*, 4728−4731.
(34) Oda, R.; Huc, I.; Homo, J.-C.; Heinrich, B.; Schmutz, M.; Candau, S. Elongated aggregates formed by cationic gemini surfactants. *Langmuir* **1999**, *15*, 2384−2390.
(35) Rogers, S.; Kohlbrecher, J.; Lettinga, M. P. The molecular origin of stress generation in worm-like micelles, using a rheo-SANS LAOS approach. *Soft Matter* **2012**, *8*, 7831−7839.
(36) Yoshizaki, T.; Yamakawa, H. Scattering Functions of Wormlike and Helical Wormlike Chains. *Macromolecules* **1980**, *13*, 1518−1525.
(37) Pedersen, J. S.; Schurtenberger, P. Scattering Functions of Semiflexible Polymers with and without Excluded Volume Effects. *Macromolecules* **1996**, *29*, 7602−7612.
(38) Pedersen, J. S.; Laso, M.; Schurtenberger, P. Monte Carlo Study of excluded volume effects in wormlike micelles and semiflexible polymers. *Phys. Rev. E: Stat. Phys., Plasmas, Fluids, Relat. Interdiscip. Top.* **1996**, *54*, R5917.
(39) Kholodenko, A. L. Analytical calculation of the scattering function for polymers of arbitrary flexibility using the Dirac propagator. *Macromolecules* **1993**, *26*, 4179−4183.
(40) Foster, T.; Safran, S. A.; Sottmann, T.; Strey, R. Scattering form factors for self-assembled network junctions. *J. Chem. Phys.* **2007**, *127*, 204711.
(41) Zilman, A.; Tlusty, T.; Safran, S. A. Entropic networks in colloidal, polymeric and amphiphilic systems. *J. Phys.: Condens. Matter* **2003**, *15*, S57−S64.
(42) Shchipunov, Y. A.; Shumilina, E. V.; Ulbricht, W.; Hoffmann, H. The branching of reversed polymer-like micelles of lecithin by sugar containing surfactants. *J. Colloid Interface Sci.* **1999**, *211*, 81−88.
(43) Pedersen, J. S. Analysis of small-angle scattering data from colloids and polymer solution: modeling and least square fitting. *Adv. Colloid Interface Sci.* **1997**, *70*, 171−210.
(44) Beaucage, G. Approximations Leading to a Unified Exponential/Power-Law Approach to Small-Angle Scattering. *J. Appl. Crystallogr.* **1995**, *28*, 717−728.
(45) Ramachandran, R.; Beaucage, G.; Kulkarni, A. S.; McFaddin, D.; Merrick-Mack, J.; Galiatsatos, V. Branch content of metallocene polyethylene. *Macromolecules* **2009**, *42*, 4746−4750.
(46) Ramachandran, R.; Beaucage, G.; Kulkarni, A. S.; McFaddin, D.; Merrick-Mack, J.; Galiatsatos, V. Persistence length of short branched polyethylene. *Macromolecules* **2008**, *41*, 9802−9806.
(47) Sorensen, C. M.; Wang, G. M. Size distribution effect on the power law regime of the structure factor of fractal aggregates. *Phys. Rev. E: Stat. Phys., Plasmas, Fluids, Relat. Interdiscip. Top.* **1999**, *60*, 7143−7148.
(48) Gerhards, R.; Jussofie, I.; Käseborn, D.; Keune, S.; Schulz, R. Modern methods for the analysis of cocoamidopropyl betaines. *Tenside Surf. Deterg.* **1996**, *33*, 8−14.
(49) https://kur.web.psi.ch/sans1/sasfit/sasfit.pdf, accessed July 2013.
(50) Magid, L. J.; Li, Z.; Butler, P. D. Flexibility of elongated sodium dodecyl sulfate micelles in aqueous sodium chloride: A small-angle neutron scattering study. *Langmuir* **2000**, *16*, 10028−10036.

DOI: 10.1021/acs.langmuir.5b01630
Langmuir 2015, 31, 8228−8234

(51) Buhler, E.; Boué, F. Chain persistence length and structure in hyaluran solutions: Ionic strength dependence for a model semirigid polyelectrolyte. *Macromolecules* **2004**, *37*, 1600−1610.
(52) Helgeson, M. E.; Hodgon, T. K.; Kaler, E. W.; Wagner, N. J. A systematic study of equilibrium structure, thermodynamics, and rheology of aqueous CTAB/$NaNO_3$ wormlike micelles. *J. Colloid Interface Sci.* **2010**, *349*, 1−12.
(53) Carale, T. R.; Blankschtein, D. Theoretical and experimental determinations of the crossover from dilute to semi dilute regimes of micellar solutions. *J. Phys. Chem.* **1992**, *96*, 459−467.

DOI: 10.1021/acs.langmuir.5b01630
Langmuir 2015, 31, 8228−8234